4-3-2007

Adaptive Time-Frequency Codes for Ultra-Wideband

Darryn Lowe
University of Wollongong, darrynl@uow.edu.au

Xiaojing Huang
University of Wollongong, huang@uow.edu.au

Adaptive Time-Frequency Codes for Ultra-Wideband

Abstract

This paper investigates inter-piconet interference (IPI) in the multi-band orthogonal frequency division multi-plexing (MB-OFDM) ultra-wideband (UWB) standard. IPI is caused when the time-frequency codes (TFCs) that delineate MB-OFDM piconets collide. An upper-bound on the severity of the IPI problem is obtained through a theoretical analysis of data-rate-specific punctured convolutional codes. Using these results, several methods for adaptive TFCs are proposed and analyzed. Comprehensive simulation results show how packet error rates (PERs) for simultaneous operating piconets (SOPs) can be improved by up to 2 dB by enabling adaptive TFCs at the transmitter. Several combinations of data rate, TFC, channel model and interferer power are studied.

Disciplines

Physical Sciences and Mathematics

Publication Details

This paper was originally published as: Lowe, D & Huang, X, Adaptive Time-Frequency Codes for Ultra-Wideband, Third International Conference on Wireless and Mobile Communications 2007 (ICWMC '07), Guadeloupe, French Caribbean, 4-9 March 2007, 38-38.

Adaptive Time-Frequency Codes for Ultra-wideband

Darryn Lowe and Xiaojing Huang
School of Electrical, Computer and Telecommunications Engineering
University of Wollongong
Wollongong, Australia, 2522
Email: {darrynl, huang}@uow.edu.au

Abstract— **This paper investigates inter-piconet interference (IPI) in the multi-band orthogonal frequency division multiplexing (MB-OFDM) ultra-wideband (UWB) standard. IPI is caused when the time-frequency codes (TFCs) that delineate MB-OFDM piconets collide. An upper-bound on the severity of the IPI problem is obtained through a theoretical analysis of data-rate-specific punctured convolutional codes. Using these results, several methods for adaptive TFCs are proposed and analyzed. Comprehensive simulation results show how packet error rates (PERs) for simultaneous operating piconets (SOPs) can be improved by up to 2 dB by enabling adaptive TFCs at the transmitter. Several combinations of data rate, TFC, channel model and interferer power are studied.**

I. Introduction

Ultra-wideband (UWB) has tremendous potential for high-rate low-power communication due to its high data rates and resistance to interference [1]. With UWB officially defined in 2002 by the United States Federal Communications Commission (FCC) as a signal with a 10 dB bandwidth of at least 500 MHz and a maximum equivalent isotropic radiated power spectral density (PSD) of no more than -41.3 dBm/MHz in the 3.1 – 10.6 GHz band [2], the race is on to exploit this untapped spectral resource.

The first UWB technology to obtain international standardization is multi-band orthogonal frequency division multiplexing (MB-OFDM) [3] developed by the WiMedia Alliance. The MB-OFDM standard [4] defines both an UWB physical layer (PHY) and medium access control (MAC) and supports data rates from 53.3 Mb/s to 480 Mb/s. MB-OFDM divides the several gigahertz of spectrum allocated by the FCC into 14 bands, each with a 528 MHz bandwidth. These bands are then bundled into 5 band groups with only the first defined as mandatory.

MB-OFDM has four distinguishing characteristics with regard to previous OFDM wireless local area network (WLAN) standards, such as IEEE 802.11a/g and HiperLAN/2. First, an MB-OFDM symbol is comprised of 128 samples rather than the 64 samples used in IEEE 802.11a. Second, a zero-pad (ZP) is used rather than a cyclic prefix (CP). Although a ZP results in higher peak-to-average power, it is more efficient than a CP since the energy of the CP is discarded by the receiver. Third, MB-OFDM supports a range of optional diversity improvements. This includes frequency domain spreading (FDS) and time domain spreading (TDS), both of which offer an extra 3 dB of process gain when activated, as well as dual carrier modulation (DCM) to combat frequency selective fading at high data rates. Fourth, time-frequency codes (TFCs) support optional time-frequency interleaving (TFI) to permit up to a 4.7 dB increase in peak transmit power. This is possible since, when each 528 MHz band is active only for 1/3 of the time, the instantaneous power can be up to 3 times higher without violating the -41.3 dBm/MHz FCC limit.

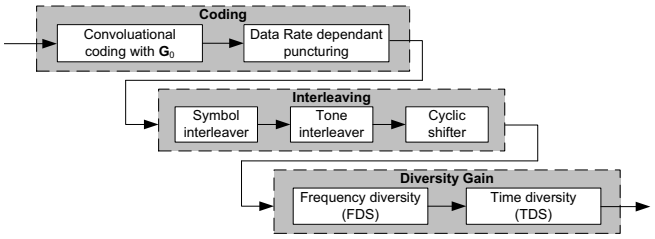

Fig. 1. Block diagram of data-rate dependent stages at MB-OFDM transmitter.

The TFCs also permit simultaneous operating piconets (SOPs). Unfortunately, since each of the independent piconets are asynchronous, it is inevitable that there will be collisions when both piconets attempt to use the same band at the same time. With high-bandwidth UWB devices ideally suited for multimedia systems, it is likely that vendor-specific proprietary networks will see multiple piconets in close proximity. As we will show, the IPI that can result from such scenarios can cripple end-to-end throughput.

This paper is organized as follows. In Section II, we quantify the severity of the IPI problem by finding the theoretical likelihood of symbol corruption resultant from TFC collision for several MB-OFDM data rates. Then, in Section III, we propose a TFC-adaptive transmitter that significantly improves performance by pro-actively detecting and avoiding symbol collisions. Section IV shows the benefits of such an approach, with Monte-carlo simulations providing PERs for several combinations of data rate, channel model, TFC and interferer power. Finally, we present our conclusions and identify future work in Section V.

II. Inter-piconet Interference

MB-OFDM enables multiple data rates through a variety of techniques. These include varying the degree of puncturing applied to the convolutional coding, the types of interleaving and optional diversity gains such as TDS and FDS. The relationships between these stages are depicted in Fig. 1 with the key parameters summarized in Table I.

Proceedings of the Third International
Conference on Wireless and Mobile Communications (ICWMC'07)
0-7695-2796-5/07 $20.00 © 2007 IEEE

Data Rate (Mb/s)	Coding Rate R	FDS	TDS Factor N_{TDS}	Coded Bits/ OFDM Symbol N_{CBPS}
53.3	1/3	Yes	2	100
80	1/2	Yes	2	100
106.7	1/3	No	2	200
160	1/2	No	2	200
200	5/8	No	2	200
320	1/2	No	1	200
400	5/8	No	1	200
480	3/4	No	1	200

TABLE I

CODING PARAMETERS FOR MB-OFDM DATA RATES.

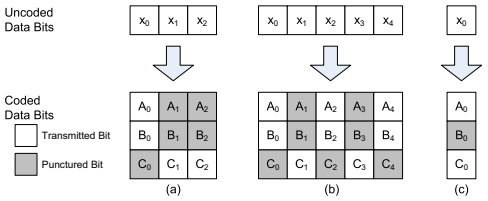

Fig. 2. Puncturing patterns for rates of (a) $\frac{3}{4}$, (b) $\frac{5}{8}$ and (c) $\frac{1}{2}$.

To quantify the robustness of a given MB-OFDM data rate to IPI, the first step is to collapse the multiple stages of the transmitter block diagram into a set of rate-specific generator matrices. Each generator matrix can then be used to obtain a rate-specific minimum free distance d_f and distance spectra c_d for $d \leq d_f$ [5].

Before we begin our analysis, we note that it is convenient to equate the lowest data rates of 53.3 and 80 Mb/s with the 106.7 and 160 Mb/s rates respectively. This incurs no loss of accuracy since the FDS is of no consequence to the coding performance in AWGN channels. In other words, although FDS improves the SNR and increases frequency diversity, the increased bit energy is achieved at the cost of doubling the packet length. This means that the noise power remains constant. Thus, since this analysis considers only AWGN channels, with consideration of frequency-selective multipath channels deferred to the Monte Carlo simulations of Section IV, the change in frequency diversity can be ignored without loss of accuracy.

All MB-OFDM data rates are derived from a single rate $\frac{1}{3}$ mother convolutional code. This code is then punctured with a rate-appropriate puncturing pattern from Fig. 2. The advantage of this approach is that, by inserting soft-decision neutral 'zeros' to replace any punctured bits, the receiver needs to consider only the mother code when implementing its Viterbi decoder [6].

To obtain single generator matrix that considers all of the stages of Fig. 1, we begin by using the *expanded generator matrices* proposed by [7] to model the impact of the data-rate dependent puncturing on the mother code. With the full derivation performed by the authors' in [8], we ultimately obtain the set of rate-specific expanded generator matrices of Table II.

The next step in our analysis is to consider the interleaving, which, in MB-OFDM, is a combination of symbol and tone interleaving with cyclic shifting and TDS. The symbol interleaving provides time-diversity by spreading successive coded bits over all six symbols in a TFC. The tone interleaving and cyclic shifting then add frequency diversity by ensuring that adjacent coded bits are mapped to maximally separated OFDM subcarriers. Finally, the TDS adds further time diversity by sending every symbol twice.

Since this analysis considers only AWGN channels, we can ignore the tone interleaving and cyclic shifting in the same way that we disregard FDS. In other words, if a given symbol in the TFC is corrupted by IPI, then *all* its coded information bits are lost. This makes the specific OFDM subcarrier that a given bit was assigned to irrelevant.

We denote the MB-OFDM interleaver as

$$y[i] = x\left[\left\lfloor \frac{i}{N_{CBPS}} \right\rfloor + \frac{6 \times \mathrm{mod}(i, N_{CBPS})}{N_{TDS}}\right] \quad (1)$$

with $i = \{0, \ldots, \frac{6N_{CBPS}}{N_{TDS}} - 1\}$ and $x[i]$ denoting the input coded information bits and $y[i]$ the interleaved output. For example, if the data rate is 320 Mb/s, where $N_{TDS} = 1$ as per Table I, the first OFDM symbol will be comprised of the coded information bits $\{x[0], x[6], x[12], \ldots, x[1194]\}$.

We denote the TDS as

$$z[j] = y\left[\left\lfloor \frac{j}{N_{CBPS}N_{TDS}} \right\rfloor N_{CBPS} + \mathrm{mod}(j, N_{CBPS})\right] \quad (2)$$

where $z[j]$ is the TDS output with $j = \{0, \ldots, 6N_{CBPS} - 1\}$. When $N_{TDS} = 1$, we observe that TDS is disabled since the expression simplifies to $z[j] = y[j]$. Alternatively, when $N_{TDS} = 2$, we see the symbol is duplicated.

To be able to revise the expanded generator matrices to consider (1) and (2), we must make two assumptions concerning the behavior of TFC collisions. First, we assume that a symbol is completely corrupted should a neighboring piconet transmit in the same band at the same time. Given that temporally overlapping OFDM symbols will suffer from increased noise over all sub-carriers, this assumption is valid so long as the power of the interfering signal is relatively high. Second, since all TFCs repeat every six symbols, we can assume that TFC collisions will be periodic. We can therefore denote a collision as forcing $z[i] = 0$ for $i = \{kN_{CBPS}, \ldots, (k+1)N_{CBPS} - 1\}$ with $0 \leq k < 6$ denoting which of the six symbols in the TFC are colliding.

We can now model TFC collisions as further puncturing. For some data rates, this will require another polyphase expansion to modify the generator matrices of Table II such that the number of columns in each matrix is an integer multiple of $\frac{6}{N_{TDS}}$. For other data rates, we will need to duplicate columns to model the TDS. The resulting *TFC-expanded generator matrices* are provided Table III, with a summary of the steps involved for each data rate following.

For the 53.3 and 106.7 Mb/s data rates, we observe that there is no need for additional polyphase expansion since the three-column generator matrix in Table II already meets the requirement that the output block size is an integer multiple of

Data Rate(s)	Input Bits	Output Bits	Puncturing Period	Generator Matrix
53.3, 106.7	1	3	1	$D^6+D^5+D^3+D^2+1 \quad D^6+D^4+D^2+D+1 \quad D^6+D^3+D^2+D+1$
80, 160, 320	1	2	1	$D^6+D^5+D^3+D^2+1 \quad D^6+D^3+D^2+D+1$
200, 400	5	8	5	$\begin{matrix} D+1 & 1 & 0 & 1 & 1 & 1 & D+1 & 1 \\ 0 & D & 1 & D & D+1 & 0 & 1 & 1 \\ D & D+1 & 1 & 0 & 1 & 1 & 0 & D+1 \\ D & 0 & D & D & D & D+1 & D & 1 \\ D^2 & D & D+1 & (D+1)\,D & 0 & 1 & D & 0 \end{matrix}$
480	3	4	3	$\begin{matrix} D^2+D+1 & D^2+1 & 1 & 1 \\ (D+1)\,D & D & D^2+D+1 & 1 \\ 0 & (D+1)\,D & D & D^2+D+1 \end{matrix}$

TABLE II

EXPANDED GENERATOR MATRICES.

Data Rate(s)	TFC-Expanded Generator Matrix
53.3, 106.7	D^6+D^5+D^3+D^2+1 D^6+D^5+D^3+D^2+1 D^6+D^4+D^2+D+1 D^6+D^4+D^2+D+1 D^6+D^3+D^2+D+1 D^6+D^3+D^2+D+1
80, 160	$\begin{matrix} 1{+}D{+}D^2 & 1{+}D{+}D^2 & 1{+}D{+}D^2 & 1{+}D{+}D^2 & 0 & 0 & 1 & 1 & 1{+}D & 1{+}D & 1 & 1 \\ D{+}D^2 & D{+}D^2 & D & D & 1{+}D{+}D^2 & 1{+}D{+}D^2 & 1{+}D{+}D^2 & 1{+}D{+}D^2 & 0 & 0 & 1 & 1 \\ 0 & 0 & D & D & D{+}D^2 & D{+}D^2 & D & D & 1{+}D{+}D^2 & 1{+}D{+}D^2 & 1{+}D{+}D^2 & 1{+}D{+}D^2 \end{matrix}$
320	$\begin{matrix} D^2{+}D{+}1 & D^2{+}D{+}1 & 0 & 1 & D{+}1 & 1 \\ D{+}D^2 & D & D^2{+}D{+}1 & D^2{+}D{+}1 & 0 & 1 \\ 0 & D & D{+}D^2 & D & D^2{+}D{+}1 & D^2{+}D{+}1 \end{matrix}$
480	$\begin{matrix} 1 & 1 & 1 & 1 & 1 & 0 & 0 & 0 & 1 & 1 & 0 & 0 \\ 0 & 0 & 1 & 1 & 1 & 1 & 1 & 0 & 1 & 0 & 1 & 0 \\ 0 & 0 & 0 & 1 & 0 & 1 & 1 & 1 & 0 & 1 & 0 & 1 \\ D & D & 0 & 0 & 1 & 1 & 1 & 1 & 1 & 0 & 0 & 0 \\ D & 0 & D & 0 & 0 & 0 & 1 & 1 & 1 & 1 & 1 & 0 \\ 0 & D & 0 & D & 0 & 0 & 0 & 1 & 0 & 1 & 1 & 1 \\ D & 0 & 0 & 0 & D & D & 0 & 0 & 1 & 1 & 1 & 1 \\ D & D & D & 0 & D & 0 & D & 0 & 0 & 0 & 1 & 1 \\ 0 & D & D & D & 0 & D & 0 & D & 0 & 0 & 0 & 1 \end{matrix}$

TABLE III

TFC-EXPANDED GENERATOR MATRICES.

$\frac{6}{N_{TDS}} = 3$. This means that we can consider the interleaver and TDS directly. Starting with the interleaver, we observe that it causes every third coded bit to be mapped to the first symbol. In other words, the first symbol will contain only the coded bits produced by the first polynomial. Further, since TDS causes each symbol to be sent twice, the second symbol will be the same as the first. The same logic applies for the remaining symbols, with symbols 3 and 4 generated by the second polynomial and symbols 5 and 6 generated by the third.

We next consider the 320 Mb/s data rate that is based on the rate $\frac{1}{2}$ code. Since this code's generator matrix has only 2 columns, we will need to use a polyphase expansion with a puncturing period of 3 to meet the minimum block size of 6. This is because the lowest common multiple (LCM) of 2, the size of the original expanded generator matrix, and 3, the result of $\frac{6}{N_{TDS}}$, is 6. Note that since the 320 Mb/s rate does not use TDS, the interleaver effectively maps each of the six columns in the TFC-expanded generator matrix to its own single symbol.

The 80 and 160 Mb/s data rates are similar to the 320 Mb/s

Indicies of Corrupted Symbols	Data Rate (Mb/s)			
	106.7	160	320	480
None	30	20	10	5
1	23	14	7	3
1 2	18	11	4	
1 2 3	15	10		
1 2 3 4	8	4		

TABLE IV

FREE DISTANCE FOR VARIOUS ERASURE CONDITIONS.

case but with the addition of TDS and FDS. Since FDS has no impact on the AWGN performance, it is not relevant to this analysis. Further, since the LCM of 2 and 3 is the same as that of 2 and 6, we observe that TDS does not impact the interleaver. This means that the only change from the 320 Mb/s case is that each column of the TFC-expanded generator matrix must be duplicated. Since the resultant matrix has 12 columns, we model each symbol that is lost due to a collision by deleting two columns. For example, a collision in the first symbol will cause an erasure of the first and seventh columns.

The final data rate we consider is 480 Mb/s. With this rate using neither TDS or FDS, a polyphase expansion by a factor of 3 is required to allow the 4 outputs of the rate $\frac{3}{4}$ expanded generator matrix to divide evenly into the 6-symbol TFCs. Since this TFC-expanded generator matrix also has 12 outputs, each symbol collision will result in the deletion of two columns in the same way as the previous case.

We do not show the TFC-expanded generator matrix for the 200 and 400 Mb/s rates since the LCM of 8, obtained from the number of columns in the expanded generator matrix of Table II and 3 is 24. Given that finding the minimum free distance of a generator matrix is an NP-complete problem [9], it is computationally infeasible to calculate the distance spectra of such a large generator matrix. Fortunately, the performance of the 200 and 400 Mb/s rates can be interpolated from the adjacent rates of 160 and 320 Mb/s and 320 and 480 Mb/s respectively. We note that although the analysis is computationally infeasible, the impractically large TFC-expanded generator matrix would still be valid.

With the relevant TFC-expanded generator matrices defined for most MB-OFDM data rates, we can now investigate the impact of TFC collisions by deleting the columns that correspond to corrupted symbols. For example, if the first symbol in a transmission at 480 Mb/s was corrupted, we would remove columns one and seven (with the left-most column denoted as column one) from the relevant TFC-expanded generator matrix.

A summary of the free distance for several MB-OFDM data rates is shown in Table IV, with a blank entry indicating that the code is catastrophic and errors are guaranteed. We observe that the high rates will be particularly sensitive to symbol collisions. For example, the 480 Mb/s rate will be barely able to recover from a single corrupted symbol. Fortunately, the lower data rates are much more robust. For example, we see that the 106.7 Mb/s rate is able to recover from the loss

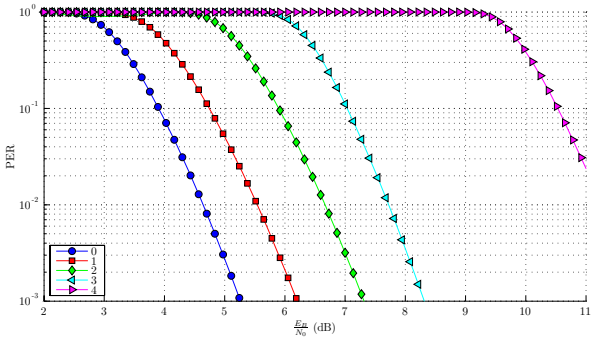

Fig. 3. Upper bound on PER with regard to number of corrupted symbols c for 160 Mb/s.

of as many as 4 out of 6 symbols. Finally, we observe that it is theoretically impossible for any code to recover from corruption of all 5 symbols, i.e. all codes at catastrophic at this point.

By considering the distance spectra c_d of a given punctured TFC-expanded generator matrix [5], we can denote the probability of a bit error as

$$P_b \leq \sum_{d=d_f}^{\infty} c_d P_d \tag{3}$$

where P_d denotes the probability of selecting the wrong path at distance d. Since all MB-OFDM constellations are based on quadrature phase shift keying (QPSK), with DCM equivalent in AWGN channels, we can denote

$$P_d = \frac{1}{2}\text{erfc}\left(\sqrt{d(6-C)\frac{E_B}{6N_0}}\right) \tag{4}$$

where E_B is the energy per information bit, N_0 is noise power spectral density and $0 \leq C \leq 6$ denotes how many of the six TFC symbols were corrupted. Note how losing a symbol reduces both the free distance of the code as well as the $\frac{E_B}{N_0}$.

Assuming that the bit errors are independent and identically distributed, which is valid for defining an upper bound, we can estimate the probability of a packet error as

$$P_p = 1 - (1 - P_b)^L \tag{5}$$

where L is the number of bits in the packet. This leads to the upperb-bound on the PER for a 160 Mb/s data rate with a 1500 octet packet shown in Fig. 3. From this example, we conclude that the combination of a rate $\frac{1}{2}$ convolutional code with TDS means that losses of up to 3 symbols incur a 1 dB loss per symbol. However, if 4 symbols are lost, the damage becomes so great that the packet is almost certain to be corrupted.

III. ADAPTIVE TFCS

In the previous section, we derived a theoretical limit on the ability of MB-OFDM to recover from IPI in the form of TFC collisions. We found that corrupted symbols degraded performance since they reduced both the effective $\frac{E_B}{N_0}$ as well as the free distance of the punctured convolutional code. In

Proceedings of the Third International
Conference on Wireless and Mobile Communications (ICWMC'07)
0-7695-2796-5/07 $20.00 © 2007 IEEE

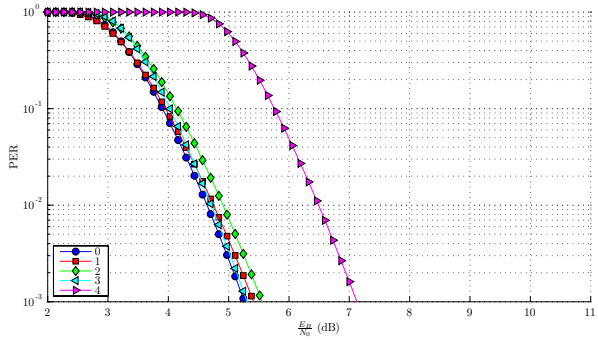

Fig. 4. Upper bound on PER with regard to number of corrupted symbols for 160 Mb/s when an adaptive transmitter is used.

TFC	Band					
1	1	2	3	1	2	3
2	1	3	2	1	3	2
3	1	1	2	2	3	3
4	1	1	3	3	2	2
5	1	1	1	1	1	1
6	2	2	2	2	2	2
7	3	3	3	3	3	3

TABLE V
TFC PATTERNS FOR BAND GROUP 1

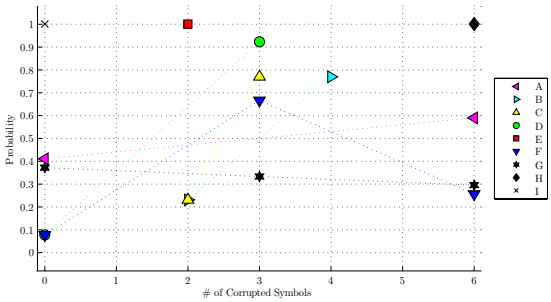

Fig. 5. Probability of symbol corruption with regard to transmitter and interferer TFC.

Transmitter TFC	Interferer TFC						
	1	2	3	4	5	6	7
1	A	B	C	D	E	E	E
2	B	A	D	C	E	E	E
3	B	F	G	C	E	E	E
4	F	B	C	G	E	E	E
5	B	B	C	C	H	I	I
6	B	B	C	C	I	H	I
7	B	B	C	C	I	I	H

TABLE VI
MAPPING OF TFC PAIR TO PROBABILITY DISTRIBUTION.

this section, we propose a technique to mitigate some of these losses by using an adaptive transmitter to skip symbols that are likely to be corrupted. The energy that was saved can then be distributed over other symbols that are less likely to suffer from IPI. Although the peak-to-average power ratio will be increased, this scheme remains FCC compliant since the average power is kept constant.

Fig. 4 demonstrates the theoretical limit of this scheme via the upper bound on PER of (5). Note that because the adaptive transmitter is not wasting energy on symbols that will be corrupted, no energy is being lost and $C = 0$. We observe that skipping 1, 2 or 3 symbols produces negligible increase to the PER at the 160 Mb/s data rate. This is a significant improvement over the original case shown in Fig. 3.

There are two complementary ways that a transmitter can implement adaptive TFCs. The first approach is to choose a fixed TFC that is least likely to suffer from interference. In other words, the transmitter would observe the environment and select its TFC to avoid conflicts with other piconets. The second approach is to dynamically adjust a TFC by skipping symbols that are likely to collide. Each of these techniques is discussed in turn.

A. Adaptive Selection of TFC

Since independent MB-OFDM piconets are not synchronized, the choice of TFC is a significant factor in determining the likelihood of symbol collisions. The 7 TFCs defined in the MB-OFDM standard are summarized in Table V. We quantify the likelihood of two TFCs colliding in Fig. 5, where we show probability distribution functions (PDFs) for the number of corrupted symbols for all combinations of local and interfering TFCs. Since some PDFs are shared by several combinations of TFCs, we enumerate all possible pairings in Table VI. For example, if we transmit on TFC 1 in an environment where TFC 3 is concurrently being used by a neighboring piconet, the probability of a symbol collision will follow PDF 'C'. This means that there will be an approximately 25% chance of a 2 symbol collision and a 75% chance of a 3 symbol collision.

Note that we define a 'collision' as when 10% or more of the total 165-sample symbol time is degraded by IPI. In other words, any OFDM symbol that has 16 or more samples of overlap with an interfering transmission is deemed to have collided. Although the 10% threshold is arbitrary, with the actual threshold of significance dependent on the relative power of the two signals, it is inconsequential here since the relative performance of the PDFs is unchanged.

These results depict three interesting points. First, we note that the PDFs are not reciprocal with regard to the transmitter and interferer TFCs. For example, a transmission on TFC 2 that is subjected to IPI on TFC 3 will behave differently than a transmission on TFC 3 subjected to IPI on TFC 2. Second, from our free distance calculations in Table IV, we would expect that any TFC combination where it is possible for 5 or more symbols corrupted will have a very high PER. This means that TFC combinations belonging to PDFs A, F, G and H will perform poorly. Of these cases, PDF F is unique since the piconet on TFC 3 will suffer much more than the piconet on TFC 2. Finally, we conclude that TFCs 1 and 2 are more robust against IPI than TFCs 3 and 4. Although TFCs 5, 6 and 7 have slightly superior PDFs, the fact that they must operate at reduced power to be FCC compliant limits their overall attractiveness.

Proceedings of the Third International
Conference on Wireless and Mobile Communications (ICWMC'07)
0-7695-2796-5/07 $20.00 © 2007 IEEE

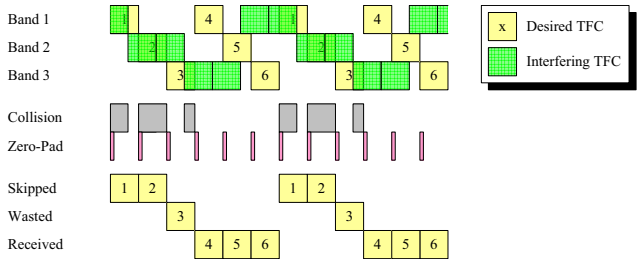

Fig. 6. Example of symbol-based IPI detection.

B. Adaptive Symbol Skipping

After a TFC is selected, the transmitter can make it dynamic by skipping symbols that will collide. The decision as to which symbols to skip depends on the degree of inter-piconet knowledge. For example, if a given transmitter has no knowledge of any interfering piconets, it is only possible for it to use a fixed TFC.

Alternatively, if a transmitter knows the scheduling of the interfering piconet, then a dynamic *packet-based* scheme may be possible. For example, this kind of system may use the clear channel assessment (CCA) time to deduce the presence of a SOP. The problem with this approach is that it forces the CCA process into a type of quasi-synchronization. In other words, the channel must evaluated for both the TFC of the intended transmission as well as any interfering ones. Since most devices will be able to operate in only one sub-band at a time, this is likely impractical.

Another more realistic option is to use a *symbol-based* scheme where we exploit the fact that a transmitter is idle for the 37 samples of zero-pad (ZP) at the beginning or end of each 165 sample symbol. If we assume that the first 5 samples of the ZP are reserved for adjusting the frequency of the local oscillator, then 32 samples remain during which the transmitter could listen to the channel for IPI.

An example of *symbol-based* detection scheme is depicted in Fig. 6, where a transmission on TFC 1 is being corrupted by IPI on TFC 3. If no action is taken, it can be readily seen that symbols 1, 2 and 3 will be lost due to collisions. However, if the transmitter could detect the interfering transmission during its ZP, it would be possible for symbols 1 and 2 to be skipped. The energy that was saved could then be used to increase the power of symbols 3 through 6 without impacting the average power. Note that symbol 3 will still be corrupted since the collision was undetectable during the ZP time. This is the weakness of symbol-based detection.

Reliable packet-based and symbol-based IPI detection will likely require that the interference be periodic. In other words, to avoid aperiodic bursts being mistaken for IPI, it may be necessary to listen for interference over several TFC repetitions. This will avoid false positives. Another variable is type of receiver processing. In other words, once the decision is made to skip some symbols, it must be decided if this will be explicitly communicated to the receiver. An example of an explicit communication would be using a preceding symbol's pilot or guard tones to indicate that the next symbol will be skipped.

IV. Results

In this section, we present results that quantify the PER of adaptive TFCs using *symbol-based* detection. These results, which consider the impact of an adaptive transmitter with regard to data rate, TFC, IPI power and channel model, are all obtained using Monte Carlo simulations. Unless otherwise specified, all packets are comprised of 1500 octets and are coded for transmission at 160 Mb/s. The default interferer power is set to 3 dB greater than that of the desired signal.

To simplify the comparison between schemes, we assume that the receiver has perfect channel state information (CSI) and implements an ideal frequency-domain equalization. Note that this does not reduce the losses due to frequency-selective fading – it simply removes channel estimation error as a complicating factor.

We also assume that the receiver estimates the noise power on a per-symbol basis. In other words, our receiver uses maximal ratio combining (MRC) with optimal weights to combine the soft-decision outputs of each demapped symbol. This per-symbol noise estimation is critical for fixed TFCs, lest even slight IPI corrupt a packet beyond repair. It is less critical for adaptive TFCs since the decision to skip as symbol could be explicitly communicated to the receiver.

A. Sensitivity to Data Rate

Fig. 7a shows the baseline PER for all data rates on TFC 1. Since this baseline has no IPI, the significant losses caused by IPI are made apparent by a comparison with Fig. 7b, which was obtained with 4 dB of IPI on TFC 6. With see that the lower data rates degraded by up to 2 dB while the 480 Mb/s rate is rendered unusable. However, when a *symbol-based* TFC-adaptive transmitter is used, the losses are greatly reduced as shown in Fig. 7c.

B. Sensitivity to TFCs

Fig. 8a shows the PER when the TFC of the IPI is changed. We see that when the desired signal uses TFC 1, that minimal IPI is obtained when the interferer uses TFCs 5, 6 or 7. This is consistent with the PDFs of Fig. 5, where it is shown that no more than $\frac{2}{6}$ symbols can be lost under these circumstances.

C. Sensitivity to Power of Interfering Piconet

Fig. 8b shows how even minor IPI can significantly increase the PER. We see that there can even be significant losses when the IPI is less than 6 dB below the desired signal. We observe again that an adaptive transmitter recovers almost all of these losses.

D. Impact of Frequency Selective Fading

Fig. 8c compares the AWGN channel and the frequency-selective CM1 channel [10]. We see that an adaptive transmitter provides over 2 dB of improvement in both multipath channels as well as AWGN.

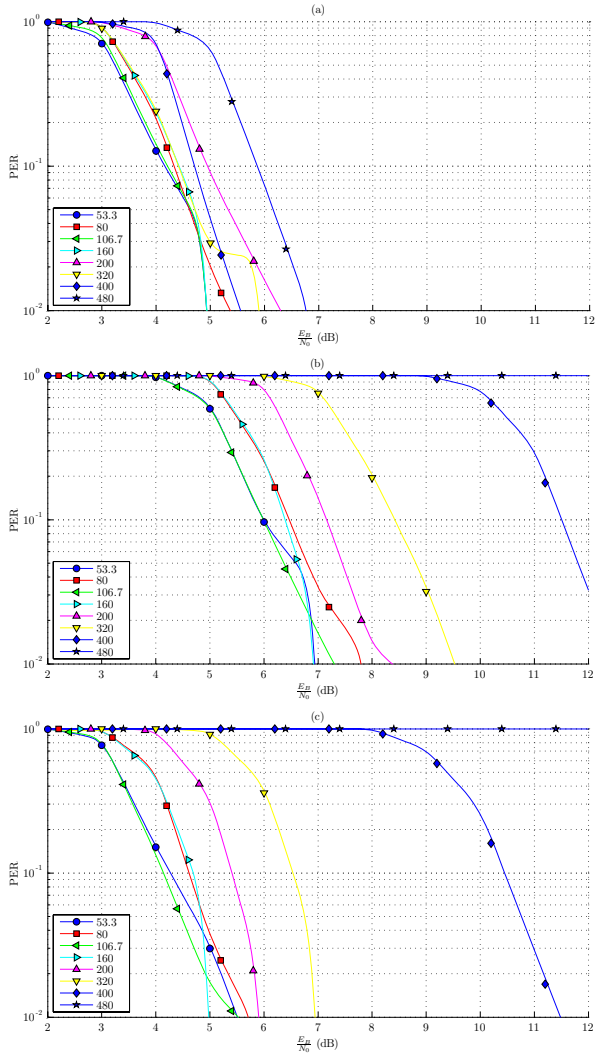

Fig. 7. (a) Baseline PER for all MB-OFDM data rates. (b) PER for all MB-OFDM data rates when degraded by inter-piconet interference. (c) With adaptive transmitter.

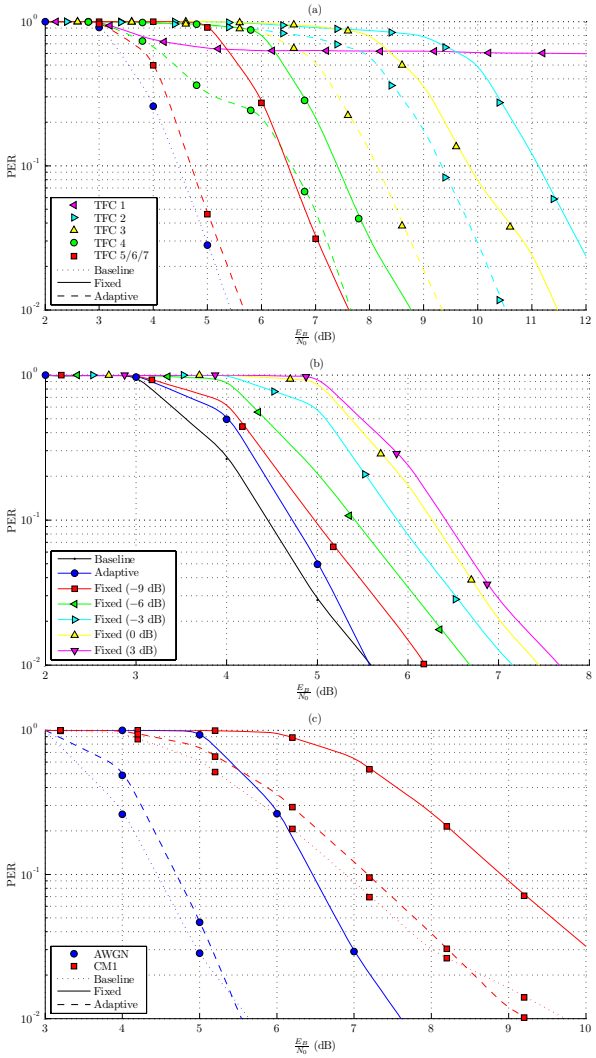

Fig. 8. PER with regard to (a) interferer TFC, (b) interferer power, and (c) channel model.

V. Conclusion

This paper presented a theoretical upper-bound on the IPI problem that can cripple SOPs in MB-OFDM UWB. An analytic framework that allows symbol collisions to be modeled as TFC-expanded generator matrices was derived. Comprehensive simulation results of a symbol-based adaptive transmitter demonstrated how the impact of IPI can be partially mitigated without adding significant computational complexity. Future work will explore specific algorithms for detecting IPI and exchanging this information between transmitters and receivers.

References

[1] K. Siwiak and D. McKeown, *Ultra-wideband Radio Technology*. Chichester, England: Wiley and Sons, 2004.

[2] *First Report and Order, Revision of Part 15 of the Commission's Rules Regarding Ultra-Wideband Transmission Systems*, Federal Communications Commission ET Docket 98-153, Feb. 2002.

[3] A. Batra, J. Balakrishnan, G. R. Aiello, J. R. Foerster, and A. Dabak, "Design of a multiband OFDM system for realistic UWB channel environments," in *IEEE Transactions on Microwave Theory and Techniques*, vol. 52, no. 9, Sept. 2004, pp. 2123–2138.

[4] *High Rate Ultra Wideband PHY and MAC Standard*, ECMA International ECMA-368, Dec. 2005.

[5] A. J. Viterbi and J. K. Omura, *Principles of Digital Communication and Coding*. New York, USA: McGrow Hill, 1979.

[6] Y. Yasuda, K. Kashiki, and Y. Hirata, "High-rate punctured convolutional codes for soft decision Viterbi decoding," *IEEE Trans. Commun.*, vol. COM-32, pp. 315–319, Mar. 1984.

[7] J. Li and E. Kurtas, "Punctured convolutional codes revisited: the exact state diagram and its implications," *UNKNOWN*, vol. UNKNOWN, pp. 2015–2019, Dec. 2004.

[8] D. Lowe and X. Huang, "Hybrid automatic repeat requests for MB-OFDM ultra-wideband," Oct. 2006, submitted to ICWMC 2007.

[9] I. Dumer, D. Micciancio, and M. Sudan, "Hardness of approximating the minimum distance of a linear code," *UNKNOWN*, vol. UNKNOWN, p. UNKNOWN, Dec. 2004.

[10] A. F. Molisch, J. R. Foerester, and M. Pendergrass, "Channel models for ultrawideband personal area networks," *IEEE Wireless Commun. Mag.*, pp. 14–21, Dec. 2003.

Proceedings of the Third International
Conference on Wireless and Mobile Communications (ICWMC'07)
0-7695-2796-5/07 $20.00 © 2007 IEEE